Digest Journal of Nanomaterials and Biostructures Vol. 16, No. 4, October-December 2021, p. 1441-1452

One-step hydrothermal synthesis and properties of CZTS/TiO_2 nanotube arrays

C. X. Zhang[a,b], Y. Gong [a], X. F. Zeng[c], B. Lu[d], H. J. Tao[c,*]
[a]*School of Materials Science and Engineering, Nanjing Institute of Technology, Nanjing 211167, China*
[b]*Jiangsu Key Laboratory of Advanced Structural Materials and Application Technology, Nanjing Institute of Technology, Nanjing, 211167, China*
[c]*College of Materials Science and Technology, Nanjing University of Aeronautics and Astronautics, Nanjing 211106, China*
[d]*Haian Hengyi Sliding Bearings Co., Ltd., Nantong 226671, China*

The large specific surface area of the tubular hollow structure of TiO_2 nanotubes provides a large number of active sites for the adsorption/catalytic reaction. With the development of the synthesis technology of nanomaterials, loading inorganic, metal and other nanoparticles on the surface of TiO_2 nanotubes has become a hot research topic in the nanomaterials field. In this paper, Cu_2ZnSnS_4(CZTS)/TiO_2 nanotube arrays composite structure was successfully prepared by one-step hydrothermal synthesis method, and the effects of different precursor concentration on the properties of the composite structure were systematically studied. The results showed that the CZTS/TiO_2 nanotubes composite sample by one-step hydrothermal synthesis achieve the highest photocurrent density which is 7 $\mu A \cdot cm^{-2}$. In addition, when the precursor solution concentration was 0.25 mmol, the sample acquired the highest photocurrent density.

(Received August 30, 2021; Accepted November 10, 2021)

Keywords: CZTS, TiO_2 nanotube arrays, Dye-sensitized solar cells, One-step hydrothermal synthesis

1. Introduction

Due to their low cost and high photoelectric conversion efficiency, dye-sensitized solar cells have become a new type of photoelectric conversion devices based on nanostructures. The current research focus is to optimize the photoanode structure to further improve the photoelectric conversion efficiency [1]. Sensitized solar cells generally consist of the following parts: sensitizer, transport material, electrode material, counter electrode and electrolyte, etc. The sensitizer generates electrons under the excitation of light. Since the conduction band of the sensitizer is generally higher than that of TiO_2, the photogenerated electrons are rapidly transferred from the sensitizer to the conduction band of semiconductor TiO_2 and FTO conductive glass, and then return to the counter electrode through the external circuit.

* Corresponding authors: taohaijun@nuaa.edu.cn

Actually, the photoanode is the carrier of dye molecules, and on the other hand, it is the channel of photogenerated electron transport, which is the core component of dye-sensitized solar cells. One-dimensional TiO_2 nanotube array shows excellent transmission performance, therefore people have done a lot of work in the TiO_2 nanotube array photoanode research [2-4], and propose many preparation methods, such as template method [5], hydrothermal method [6] and anodic oxidation method [7]. Among these preparation methods, the template method and anodic oxidation method are the most widely used because of their simple preparation, good repeatability and adjustable pipe diameter and length. However, TiO_2 nanotube sensitized solar cells still have several shortcomings: (1) Low specific surface area affects the dye adsorption capacity; (2) TiO_2 nanotubes crystallized after treatment are usually composed of anatase structure with lower active surface. The two aspects cause the low photoelectric conversion efficiency.

At present, thin-film photovoltaic technologies such as copper indium selenium (CIS), copper indium gallium selenium (CIGS) and cadmium, tellurium (Cd, Te) still need further improvement, as they rely on expensive rare earth elements (In, Ga, Te) and toxic elements (Cd) in the earth's crust, and the price, availability and toxicity of the materials are growing concerns. Therefore, in the future, in order to reduce costs and increase production, we should rely on elemental rich and non-toxic compounds [8]. Quaternary semiconductor Cu_2ZnSnS_4 (CZTS) is a promising absorber material for solar cell with low cost, abundant content, low toxicity, a band gap of 1.45-1.51 eV and high light absorption coefficient (>104 cm^{-1}) [9]. The theoretical power conversion efficiency (PCE) of CZTS solar cells is about 30% [10]. Various methods have been developed to deposit CZTS films, including sputtering deposition [11-13], vacuum thermal evaporation [14], electron beam evaporation [15], spray pyrolytic deposition, sol–gel deposition, electrodeposition, photochemical deposition, pulsed laser deposition, screen-printing, and nanoparticle-based method [16].

In this paper, TiO_2 nanotube arrays were first prepared by anodic oxidation method. On this basis, they were subjected to heat treatment crystallization or hydrothermal crystallization, and hydrothermal loading of CZTS. The effects of different synthesis methods on the composite structure morphology, microstructure and photochemical properties of CZTS/TiO_2 nanotubes were systematically analyzed in the three-electrode system. The effect of different precursor concentrations on the composite structure of CZTS/TiO_2 nanotubes was studied by one-step hydrothermal synthesis method. CZTS replaced the sensitized dyes in TiO_2 DSSC. P-type CZTS are like absorbers that generate carriers through absorption and light, similar to organic or organometallics, and the CZTS/TiO_2 structure exhibits photovoltaic properties.

2. Experimental

The pure titanium foil used in the experiment was 0.25 mm thick and 99.6 % pure (purchased from Baoji Jiuding Titanium Products Factory). The size of the platinum electrode used for the anodic oxidation reaction is 20 mm×30 mm×0.2 mm, and the purity is 99.99 % (purchased from Beijing General Research Institute for Nonferrous Metals). A counter electrode used for battery assembly is a Pt/FTO electrode with a size of 180 mm×30 mm×3.2 mm (purchased from Dyesol company in Australia). The reagents used in the experiment, such as ethanol (CH_3CH_2OH), hydrofluoric acid (HF), copper acetate monohydrate [$Cu(CH_3COO)_2 \cdot H_2$], zinc acetate

[$Zn(CH_3COO)_2 \cdot 2H_2O$], copper chloride ($CuCl_2 \cdot 2H_2O$), stannous chloride ($SnCl_2 \cdot 2H_2O$) and zinc chloride ($ZnCl_2$), were all produced in Nanjing Chemical Reagent Co., Ltd. Thiourea (H_2NCSNH_2), tin chloride (H_2NCSNH_2) manufacturers for the Sinopharm Group.

Anodic oxidation method is an electrochemical method to prepare TiO_2 nanotube arrays in low concentration electrolyte solution, such as ammonium sulfate and ammonium fluoride. Due to the fact that TiO_2 nanotube arrays are grown vertically on Ti substrates, it is easy to make devices and can be recovered, and the anodic oxidation method has become an effective and low-cost method for preparing TiO_2 nanotube arrays [17]. In the experiment, pure titanium foil (1 cm × 1 cm) was used as the substrate. Before the reaction, the samples were subjected to acetone ultrasonic oil removal and chemical polishing successively, and the polishing liquid composition was HF: HNO_3: H_2O = 1: 1: 2 (volume ratio), and then washed with distilled water to be used. At room temperature (about 25 ℃), the titanium foil was anodized in an aqueous solution of 0.5 wt.% HF using platinum sheet as counter electrode. The oxidation voltage is 20 V, the oxidation time is 30 min, and the distance between the poles is kept at 3 cm. After the reaction is completed, the sample is soaked in distilled water and washed, and then dried by cold air.

Generally, TiO_2 nanotube arrays prepared by anodic oxidation are amorphous and need to be crystallized by heating treatment at high temperature (>400 ^oC). However, the high temperature crystallization not only causes the thickening of the barrier layer, which leads to the increase of the resistance, but also causes the collapse of the nanotube structure and the decrease of the adhesion with the matrix. The low temperature crystallization routes of TiO_2 nanotube arrays have attracted attention [18-19], such as the anodic oxidation followed by hydrothermal crystallization. Crystallization of TiO_2 nanotube arrays by heat treatment: the anodized titanium foil samples were placed on Al_2O_3 ceramic sheets and heating treated in a box-type high-temperature sintering furnace. The heating treatment process was controlled by program. The temperature was raised at a speed of 5 $^oC \cdot min^{-1}$, and when the temperature reached 350 ℃, the samples were kept for 3 h and then cooled with the furnace. Crystallization of TiO_2 nanotube arrays by hydrothermal treatment: water treatment is put after anodic oxidation of the sample in a volume of 50 ml of stainless steel in the reaction kettle, the tank is made of PTFE material, add 40 ml of distilled water, make the filling rate of 80 %, after the reaction kettle tight into the oven, under the temperature 180 ℃ for 2 hours, then cool to room temperature naturally take out samples, rinse clean with distilled water, and dry at low temperature.

The composite structure of CZTS/TiO_2 nanotubes was obtained by one-step hydrothermal loading CZTS particles on the prepared TiO_2 nanotubes. The process is as follows: (1) CZTS hydrothermal precursor configuration: a certain amount of copper chloride, zinc chloride, stannous chloride and thiourea were dissolved in 35 mL distilled water at a 2:1:8 molar ratio, and then transferred to the PTFE lining with a volume of 50 mL after complete dissolution. (2) TiO_2 nanotube array is fixed in the reactor: the TiO_2 nanotube array prepared by anodic oxidation is placed at the bottom of the lining containing the precursor solution, and the lining is put into the stainless-steel reactor. (3) Heating reaction kettle: put the reaction kettle into the oven after tightening, adjust the temperature to 200 ^oC and hold for 24 h. (4) The final sample was obtained: after the reaction, the sample was naturally cooled to room temperature, washed with distilled water, and dried at low temperature.

The surface of TiO_2 nanotubes array was washed with anhydrous ethanol and dried at low temperature. Then, TiO_2 nanotube array sensitized by CZTS was fixed on the slide, and an

appropriate amount of multi-sulfur electrolyte (The electrolyte is prepared by weighing 2.400 g of Na_2S, 0.640 g of S and 0.149 g of KCl, dissolving in 10 mL of water /methanol mixture with a volume ratio of 3: 7, and stirring until orange solution is formed) was added, and the FTO counter electrode (The surface of TiO_2 oxide film is opposite to Pt layer of FTO) was quickly affixed. Finally, clips are attached to both ends, and the battery is prepared. The morphology of the samples was characterized by Hitachi S4800 field emission scanning electron microscope (FE-SEM) and FEI Tecnai G2 T20 Transmission Electron Microscope (TEM). The crystal structure was characterized by Bruker D8 ADVANCE X-ray diffractometer (XRD), HORIBA Jobin Yvon LabRAM HR high resolution microscopic Raman spectrometer (Raman) and selective electron diffraction patterns in transmission electron microscopy (SAED). The photochemical properties of CZTS/TiO_2 nanotube composite films were tested using a standard three-electrode system. Among them, the sample is the working electrode, the platinum electrode is extremely auxiliary electrode, and the saturated calomel electrode (SCE) is the reference electrode (all the potential mentioned in the paper are relative to the reference electrode). Then, each electrode was put into a quartz beaker containing 0.5 mol·L^{-1} Na_2SO_4 aqueous solution, and connected to an electrical chemistry workstation (Shanghai Chen Hua Instrument Company CHI660D) to record the photocurrent response curve and photocurrent densities - potential curve of the sample. The light source is Oriel's 1000W Class B Full Spectral Solar Simulator (Type 91192), which illuminates the working electrode surface with an intensity of 70 mW·cm^{-2} and an effective light area of 1 cm^2.

3. Results and Discussion

In HF aqueous system, TiO_2 nanotube arrays were obtained by anodic oxidation method, on the basis of different synthesis methods on CZTS/TiO_2 morphology was studied, the influence of the microstructure and performance, by step hydrothermal synthesis of CZTS/TiO_2 nanotube composite structure, different concentration of precursors (0.05 mmol, 0.1 mmol, 0.25 mmol, 0.5 mmol) influence on CZTS/TiO_2 nanotube composite structure.

In this part, the TiO_2 nanotube array is crystallized in different ways, and the influence of the synthesis method on the composite structure of CZTS/TiO_2 nanotubes is studied.

Fig. 1 shows the FE-SEM diagram of the composite structure of CZTS/TiO_2 nanotubes prepared by different synthesis methods. The morphology of TiO_2 nanotube arrays after heating treatment at 350 ^oC is shown in Fig. 1(a). The nanotube arrays are orderly arranged with clear morphology. After 24 h of hydrothermal treatment, new phase CZTS gather and grow along the tube orientations, even blocking part of the tube orientations, as shown in Fig. 1(b). The morphology of the hydrothermal crystallized nanotube array is granular accumulation, as shown in Fig. 1(c). After hydrothermal treatment in the precursor of CZTS, CZTS crystals are loaded in the TiO_2 granular void and surface. These nanorods are about 100 nm in length and 20 nm in diameter, and disperse irregularly on the TiO_2 surface, as shown in Fig. 1(d). The CZTS /TiO_2 nanotube composite structure was synthesized by hydrothermal synthesis in one step, and the particles on the sample surface were distributed uniformly without particle aggregation, maintaining the hollow structure of the nanotubes before the reaction, as shown in Fig. 1(f).

This indicates that the surface of TiO_2 nanotube array films with different crystallization treatments is hydrothermally loaded with different morphologies of CZTS, and the CZTS/TiO_2

composite structure with different morphologies is obtained.

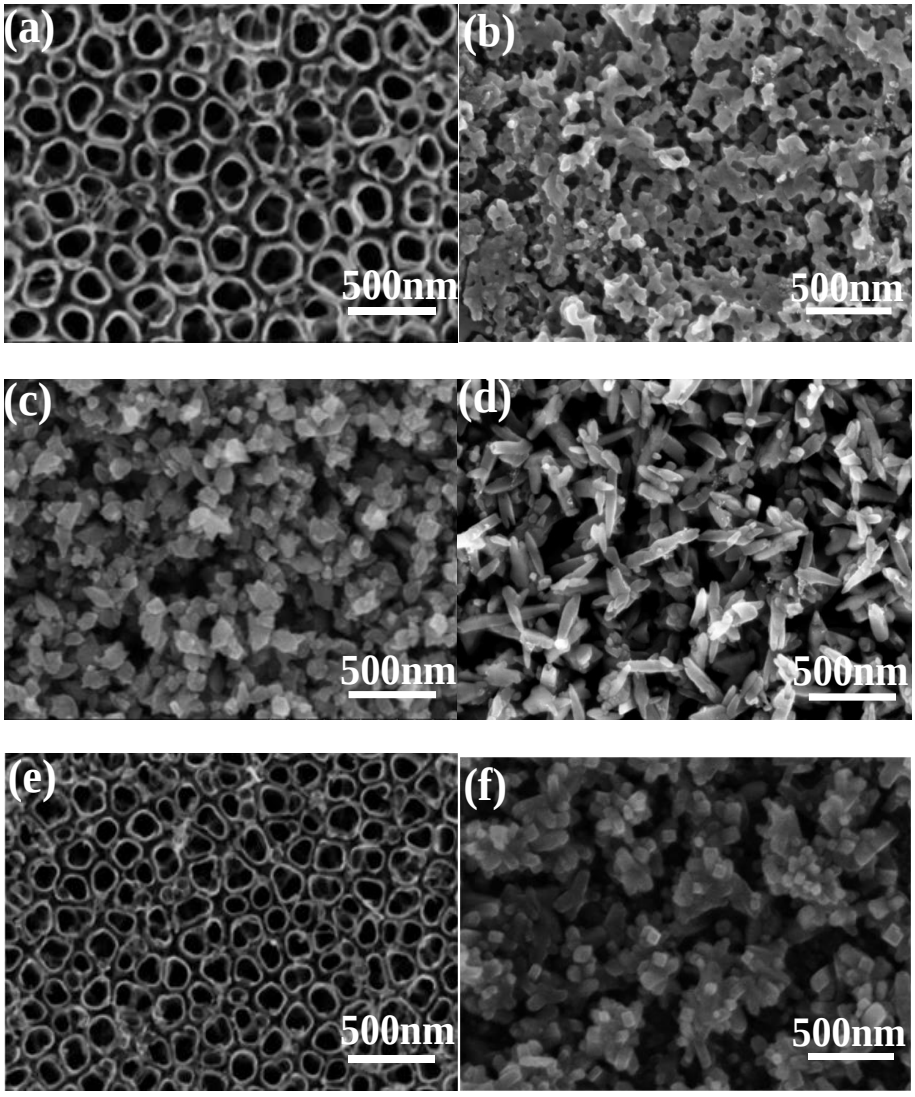

Fig. 1. Influence of synthesis method on morphology of CZTS/TiO_2 (a and b) Heat treatment crystallization and hydrothermal deposition, (c and d) hydrothermal crystallization and hydrothermal deposition, (e and f) one-step hydrothermal synthesis.

Fig. 2 shows XRD patterns of CZTS/TiO_2 composite structures prepared by different synthetic methods. It can be seen from the figure that the anatase phase characteristic diffraction peaks of each sample appear at 25^o and 48^o, indicating that the TiO_2 nanotube array has achieved good crystallization effect in the early crystallization treatment. In this part, the TiO_2 nanotube array is crystallized in different ways, and the influence of the synthesis method on the composite structure of CZTs/TiO_2 nanotubes is studied.

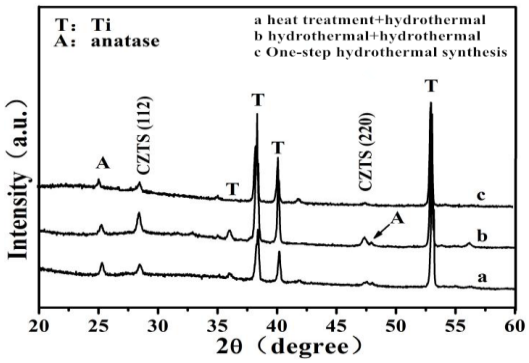

Fig. 2. XRD patterns of CZTS /TiO_2 composite structures prepared by different synthesis methods.

In order to further explain that the prepared product is CZTS/TiO_2 composite structure, Raman spectroscopy was also adopted to analyze the above samples (as shown in Fig. 3). In the Raman spectra of each sample, only the characteristic vibration peaks of anatase phase TiO_2 and zincxanthite CZTS were found, and no characteristic vibration peaks of other sulfides were found. This result was consistent with the content expressed in Fig. 2.

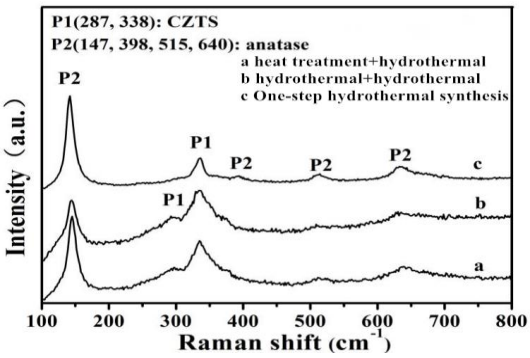

Fig. 3. Raman spectra of CZTS/TiO_2 prepared by different synthetic methods.

XRD spectra and Raman spectra show that the anodized TiO_2 nanotube array after heat treatment and hydrothermal treatment respectively, the hydrothermal method can successfully load pure phase CZTS in the tube array, so as to prepare the heterozygous CZTS/TiO_2 composite structure.

As can be seen from the figure, in the dark state, the photocurrent density of each electrode is very small, almost zero. At the moment of illumination, the current spike appeared, however the photocurrent reached a stable state after a short period, and the current value did not change much after 3 cycles, indicating that each electrode had good photocurrent stability [20].

Crystallization heat treatment of the hydrothermal synthesis of TiO_2 nanotubes CZTS/TiO_2 nanotubes composite electrode results in the low current density is, about 5 $\mu A \cdot cm^{-2}$ (Fig. 4a). This is because in the composite structure of CZTS/TiO_2 nanotubes of the electrode, CZTS clumped together at the edge of the TiO_2 nanotube orientations and blocked most orientations of the tubes, resulting in small specific surface area of the electrode and fewer photochemical active sites, so the photocurrent density obtained is low. TiO_2 nanoparticles loaded CZTS nanorods hydrothermal

crystallization of the sample (Fig. 4b) and one-step hydrothermal synthesis of CZTS/TiO_2 nanotubes composite sample (Fig. 4c) has a relatively high specific surface area, and achieved the high photocurrent density, respectively, 6 μA·cm^{-2} and 7 μA·cm^{-2}.

In addition, it is not difficult to find that electrode c obtains a higher photocurrent density than electrode b. This is because the nanotube array structure is relatively intact through the one-step hydrothermal synthesis method, which provides a high-speed channel for the transmission of photogenerated electrons to the titanium matrix, thus effectively reducing the recombination of photogenerated electrons and holes and increasing the number of photogenerated carriers.

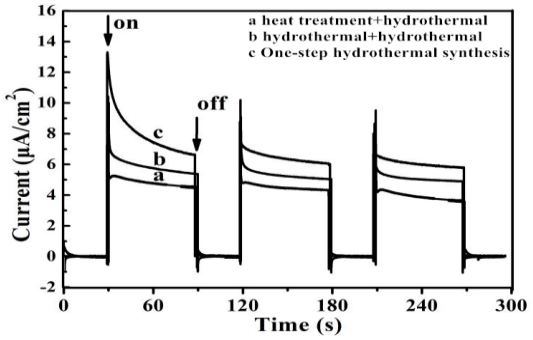

Fig. 4. Transient photocurrent spectra of CZTS /TiO_2 prepared by different synthesis methods.

Fig. 5 shows the XRD patterns of anodized TiO_2 nanotube arrays after hydrothermal treatment in different concentrations of precursor solution for 24 h. As can be seen from the figure, the (112) crystal plane characteristic diffraction peak of zinc-yellow tin type CZTS appears in each sample at 28.5° [PDF # 26-0575]. The intensity of diffraction peak increases with the increase of precursor concentration. In addition, the characteristic diffraction peak of CuS was also found in the samples with low concentration (x=0.05 mmol, x=0.1 mmol) precursor hydrothermal treatment, indicating that the hydrothermal reaction was not sufficient when the precursor concentration was too low, resulting in the occurrence of heterogeneous CuS. In addition, the characteristic diffraction peaks of TiO_2 anatase phase appear in all samples at 25° and 48°, indicating that the amorphous TiO_2 nanotube array is crystallized while hydrothermal loading CZTS.

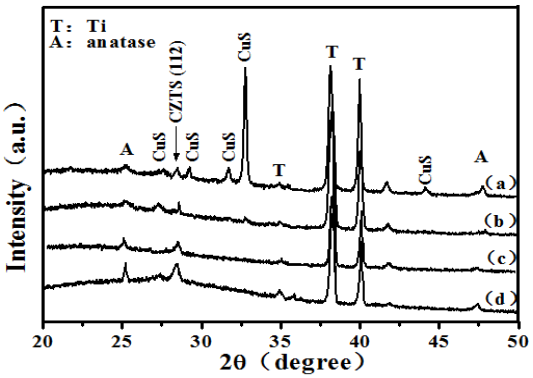

Fig. 5. XRD pattern of CZTS/TiO_2 nanotube composite structure synthesized by hydrothermal method with different concentrations of precursor solution (a) x=0.05 mmol, (b) x=0.1 mmol, (c) x=0.25 mmol, (d) x=0.5 mmol.

The ZnS pattern of the cubic crystal [PDF # 05-0566] is similar to that of the CZTS crystal, and it is difficult to distinguish the both by XRD. In order to further explain that the sample synthesized by hydrothermal method is CZTS/TiO_2 composite structure, Raman spectroscopy was used to analyze the sample.

Fig. 6 is the Raman spectrum of hydrothermal samples with precursor concentration x= 0.25 mmol and x= 0.05 mmol. As shown in Fig. 6 (a), unimodal P1 is the vibration mode of CZTS sulfur atom at 338 cm^{-1} of zinc yellow tin ore, which is consistent with the results reported by Kushp et al [21-22]. While the longitudinal optical phonon model (LO) of ZnS is located at 350 cm^{-1} [23], Raman spectroscopy clearly distinguishes CZTS from ZnS. At the same time, the characteristic vibration peaks of anatase TiO_2 at 147 cm^{-1}, 400 cm^{-1}, 515 cm^{-1} and 640 cm^{-1} were also found at P2, and 147 cm^{-1} was the strongest vibration peak of anatase TiO_2. Fig. 6(a) and fig. 5(c) show that CZTS/TiO_2 composite structure without impurity phase was successfully prepared by hydrothermal method in precursor solution with concentration of x= 0.25 mmol for 24 h. A characteristic vibration peak with CuS at 470 cm^{-1} [24] appears in the hydrothermal sample with concentration x= 0.05 mmol (as shown in Fig. 6b), which is consistent with the results of XRD Fig. 5(a).

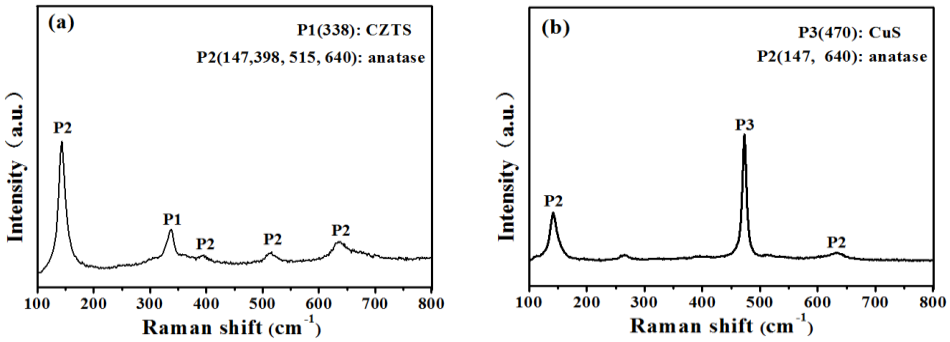

Fig. 6. Raman spectra of CZTS/TiO_2 nanotube composite structure synthesized by hydrothermal reaction of precursors at different concentrations (a) x= 0.25 mmol, (b) x= 0.05 mmol.

Hydrothermal treatment will change the TiO_2 nanotube array structure into a film layer of particle accumulation. Fig. 7 is the FE-SEM diagram of the CZTS/TiO_2 nanocomposite structure in precursor solution with different concentrations. It can be found from the figure that newly generated CZTS and hybrid CuS particles are mixed with TiO_2 particles, which cannot be clearly distinguished by FE-SEM. Comparatively speaking, the surface particle distribution of the hydrothermal sample with a concentration of x=0.25 mmol was relatively uniform, and there was no particle aggregation (Fig. 7c).

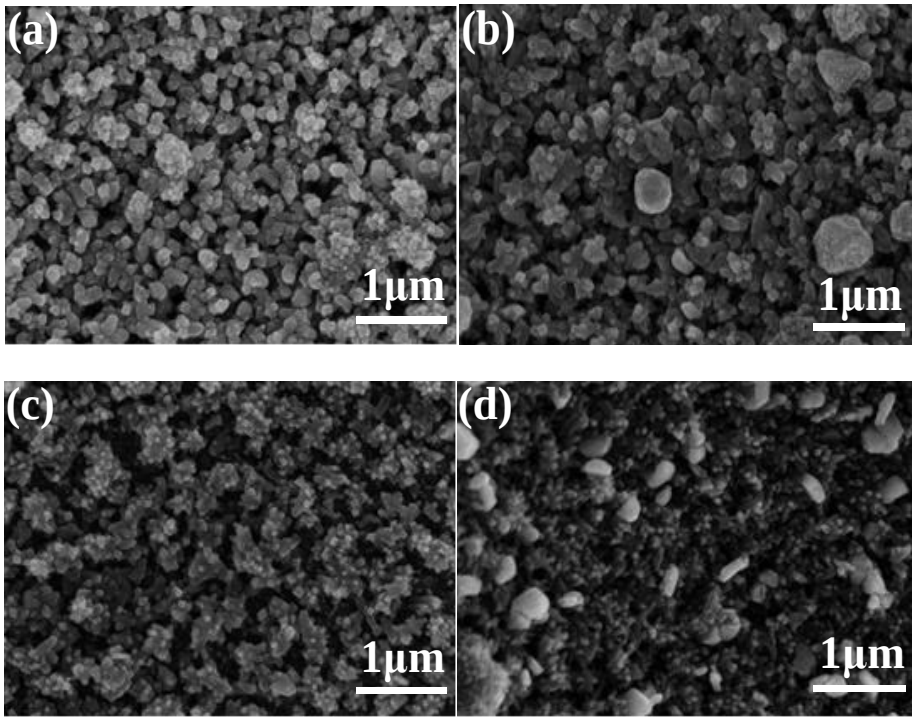

Fig. 7. FE-SEM diagram of CZTS/TiO_2 nano-composite structure synthesized by hydrothermal method with different concentrations of precursor solution (a) x=0.05 mmol, (b) x=0.1 mmol, (c) x=0.25 mmol, (d) x=0.5 mmol.

Fig. 8 shows the transient photocurrent time curve of CZTS/TiO_2 nanotube composite electrode hydrothermal synthesis of precursor solution with different concentrations in 0.5 mol·L^{-1} Na_2SO_4 solution, 70 mW·cm^{-2} simulated solar light, applied voltage at zero. As can be seen from the figure, when there is no light, the photocurrent density of each electrode is almost zero. When the light is illuminated, the photocurrent is generated instantaneously, and after a short period, the photocurrent reaches a stable state, indicating that each electrode has a good photocurrent stability. When the precursor solution concentration is 0 mmol, the hydrothermal sample is shown in Fig. 8(a), and its current density is about 2.7 μA·cm^{-2}. This is because TiO_2 without CZTS sensitization responds only to visible light region and produces very few photogenerated carriers. In contrast, the hydrothermal samples with precursors (Fig. 8b-e) obtained a higher photocurrent density. In addition, it is not hard to find that electrode d acquired obviously higher photocurrent density, about 6 μA·cm^{-2} than electrode b, c, e. This is because the CZTS/TiO_2 composite structure synthesized by x=0.05 mmol and x=0.1 mmol has heterophase CuS, CuS is a kind of conductive phase, and its existence intensifies the probability of carrier recombination, thus reducing the photochemical properties of the electrode. However, there are a few large particles on the surface of CZTS/TiO_2 composite structure synthesized by x=0.5 mmol, which is not as many active sites as the sample with uniform morphology of x=0.25 mmol, and its photochemical properties are relatively poor. In the figure, each electrode generates photocurrent at the moment of illumination, however there is a current spike. This is because in the absence of external bias, the photoelectrons and holes compound before they have time to transmit at the beginning of illumination.

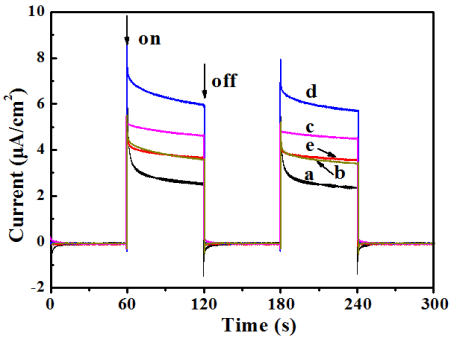

Fig. 8. Photocurrent response of CZTS /TiO_2 nanotube composite electrode prepared by hydrothermal synthesis of precursors with different concentrations (a) x=0 mmol, (b) x=0.05 mmol, (c) x=0.1 mmol, (d) x=0.25 mmol, (e) x=0.5 mmol.

It can be seen from the fig. 9 that with the increase of applied voltage, the electric field intensity increases, which is not only conducive to the separation of electrons and holes, but also reduces the recombination of electrons and solution. It can be seen from the figure that electrode a has a low photocurrent density, while electrode b-e loaded with CZTS has a relatively high photocurrent density. This is because loading CZTS particles onto TiO_2 not only extends the optical response range of TiO_2 to the visible region [25], but also improves the separation efficiency of photogenerated electron-hole. Among them, the photocurrent density of electrode b and c decreases locally with the increase of electrode potential. This is because there is a conductive hybrid phase between the two electrodes. When the electrode potential increases, photoelectrons are more likely to gather here and recombine.

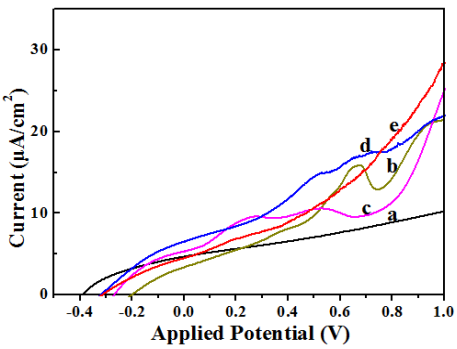

Fig. 9. Photocurrent density-potential curve of CZTS /TiO_2 composite electrode prepared by hydrothermal synthesis of precursors with different concentrations (a) x=0 mmol, (b) x=0.05 mmol, (c) x=0.1 mmol, (d) x=0.25 mmol, (e) x=0.5 mmol.

4. Conclusions

In this paper, the composite structure of CZTS/TiO_2 nanotubes was successfully prepared by one-step hydrothermal method, and its morphology, microstructure and photochemical properties were studied.

The multiphase carbon free nanotubes/titanium dioxide nanotubes composite structure was synthesized by hydrothermal treatment (x=0.25 mmol, 24 h) of different crystallization methods. In contrast, CZTS/TiO_2 nanotubes synthesized by one-step hydrothermal method have more uniform particle distribution on the sample surface, and the hollow structure of nanotubes is beneficial to improve the photoelectric performance.

The CZTS/TiO_2 nanotube composite structures were synthesized by one-step hydrothermal method (200 ℃, 24 h) in different concentrations of precursor solutions. It was found that the CZTS/TiO_2 composite structures doped with CuS were easily obtained in low concentrations of precursor solutions, and the photochemical properties of the composite structures were low. When the precursor concentration x=0.25 mmol, the CZTS/TiO_2 composite structure does not contain impurity phase, the morphology is uniform, more active sites are obtained, and has good photochemical properties.

Acknowledgements

The support by the National Natural Science Foundation of China (22005144, 51372115, 11575084), the Opening Project of Jiangsu Key Laboratory of Advanced Structural Materials and Application Technology (ASMA201911), the Key R & D Plan of Jiangsu Province (Competitive Project, BE2018091).

References

[1] K. Arifin, R. M. Yunus, L. J. Minggu, M. B. Kassim, Int. J. Hydrogen. Energ. **46**, 4998 (2020).
[2] M. Yang, D. Kim, H. Jh, K. Lee, J. Paul, P. Schmuki, Chem. Commun. **47**, 2032 (2011).
[3] Q. Wang, S. Li, J. Qiao, R. Jin, Y. Yu, S. Gao, Sol. Energ. Mat. Sol. C **132**, 650 (2015).
[4] N. Sriharan, N. Muthukumarasamy, T. S. Senthil, M. Kang, J. Sol-Gel. Sci. Techn. **85**, 743 (2018).
[5] H. Wang, Y. Song, W. Liu, S. Yao, W. Zhang, Mater. Lett. **93**, 319 (2013).
[6] L. Li, J. Ya, L. Xiang, Z. Liu, E. Lei, Appl. Phys. A **123**, 667 (2017).
[7] M. Wu, H. Wei, Y. Wei, A. Yao, J. Bu, J. Lin, Z. Dong, Y. Chen, Y. Cui, Z. Wu, Vib. Spectrosc. **95**, 32 (2018).
[8] J. Lopez, G. Pérez, J. Cuaspud, E. López, Y. P. Triana, ECS Trans. **100**, 85 (2021).
[9] E. K. Michael, D. Norcini, S. Komarneni, J. Brownson, Ceram. Int. **39**, 7935 (2013).
[10] P. S. Jitendra, B. Rohidas, J. Solid. State. Electr. **24**, 461 (2020).
[11] S. Zhuk, A. Kushwaha, T. Wong, S. Masudy-Panah, A. Smirnov, G.K. Dalapati, Sol. Energ. Mat. Sol. C **171**, 239 (2017).
[12] T. Srinivasan, D. Jovina, A. Rajesh, Sol. Energy **106**, 166 (2014).
[13] S. A. Vanalakar, G. L. Agawane, S. W. Shin, M. P. Suryawanshi, K. V. Gurav, K. S. Jeon, P. S. Patil, C. W. Jeong, J. Y. Kim, J. H. Kim, J. Alloy Compounds **619**, 109 (2015).
[14] K. C. Sekhar, S. L. Abhilasha, S. R. Bhat, N. U. Raj, K. Srikrishna, K. Gopal, R. G. K. Urs, R. Nagapadma, IOP Conference Series: Mater. Sci. Eng. **402**, 012138 (2018).

[15] E. M. Mkawi, Y. Al-Hadeethi, E. Shalaan, E. Bekyarova, J. Mater Sci: Mater Electron. **29**, 20476 (2018).
[16] L. Li, B. Zhang, M. Cao, Y. Sun, J. Jiang, P. Hu, Y. Shen, L. Wang, J. Alloy. Compound. **551**, 24 (2013).
[17] S. Wu, S. Wang, W. Liu, X. Yu, D. Wen, Surf. Coat. Tech. **374**, 362 (2019).
[18] S. B. Nair, A. John, S. S. Menon, H. Rahman, J. A. Joseph, S. Shaji, R. R. Philip, Semicond. Sci. Tech. **34**, 095023 (2019).
[19] S. B. Nair, A. John K, J. A. Joseph, S. Shaji, R. R. Philip, Mater. Today.: proceedings **25**, 203 (2020).
[20] M. Majid, R. Sohrab, E. Mohammadreza, B. Reza, N. Mohammad, Int. J. Hydrogen. Energ. **46**, 21475 (2021).
[21] P. Kush, S. Deka, J. Nanopart. Res. **16**, 1 (2014).
[22] H. R. Jung, S. W. Shin, M. P. Suryawanshi, S. J. Yeo, H. K. Jin, J. H. Yun, J. H. Moon, J. H. Kim, Sol. Energy. **145**, 2 (2016).
[23] C. A. Arguello, D. L. Rousseau, S. P. S. Porto, Phys. Rev. **181**, 1351 (2015).
[24] B. Minceva-Sukarova, M. Najdoski, I. Grozdanov, C. J. Chunnilall, J. Mol. Struct. **410**, 267 (1997).
[25] M. Sun, Y. Yao, Z. Zhang, B. Gao, W. Ding, Int. J. Hydrogen. Energ. **45**, 21493 (2020).